## **Supplementary Materials**

## Stretchable zipper

Fanming Wang<sup>1,2</sup>, Qinlan Li<sup>1,2</sup>, Zhitong Wang<sup>3</sup>, Yewang Su<sup>1,2,\*</sup>

<sup>1</sup>State Key Laboratory of Nonlinear Mechanics, Institute of Mechanics, Chinese Academy of Sciences, Beijing 100190, China.

<sup>2</sup>School of Engineering Science, University of Chinese Academy of Sciences, Beijing 100049, China.

<sup>3</sup>Wide Range Flight Engineering Science and Applications Center, Institute of Mechanics, Chinese Academy of Sciences, Beijing 100190, China.

\*Correspondence to: Prof. Yewang Su, State Key Laboratory of Nonlinear Mechanics, Institute of Mechanics, Chinese Academy of Sciences, Beijing 100190, China. E-mail: yewangsu@imech.ac.cn

#### **MAIN TEXT**

# Supplementary Text 1. Calculation of the critical strain for dividing different initial contact conditions.

Depending on different tape strains, the initial contact conditions between teeth exhibit corresponding distinctions, leading to discrepancies in the interlock process. Taking Supplementary Figure 2 as an example, the difference is first manifested in whether  $B_3$  is in contact with  $A_3$  while contacting  $A_2$ . Evidently, under the condition that  $\varepsilon_2$  remains constant, as  $\varepsilon_1$  gradually decreases; the distance between  $B_3$  and  $A_3$  will decrease until mutual contact is established. Analyzing the tape strain at the moment when the contact between  $B_3$  and  $A_3$  occurs yields the following system:

$$\begin{cases}
\left[T - L\sin\theta + L\sin(\theta + \varphi)\right]^{2} + \begin{bmatrix} T_{3} - \left(L\cos\theta - T_{1}\sin\theta\right) + \\ \left(A + d_{1}\right)\sin\theta - \\ \left(L\cos\left(\theta + \varphi\right) + T_{2}\sin\left(\theta + \varphi\right)\right) \end{bmatrix}^{2} - \left(2R\right)^{2} = 0 \\
\left[T_{4} - T - L\sin\left(\theta + \varphi\right) + L\sin\theta\right]^{2} + \begin{bmatrix} T_{5} - L\cos\theta - \\ L\cos\left(\theta + \varphi\right) \end{bmatrix}^{2} - \left(2R\right)^{2} = 0
\end{cases}$$
(S1)

where  $T = (A + d_1 - T_1)\cos\theta - T_2\cos(\theta + \varphi)$  is the horizontal distance between the centroid of the posterior surface of B<sub>3</sub> and the turning point of the track,  $A = \varepsilon_2 W - (L + R)\sin(\theta/2)$  represents the distance between the edge of the posterior surface of B<sub>2</sub> and B<sub>3</sub>,  $d_1 = 2.2$ mm is the track-directional distance from the edge of the posterior surface of B<sub>3</sub> to the rotation axis O<sub>2</sub>,

 $T_1 = W - \left[ \left( L + R/2 \right) \tan \theta + \left( 1 - \varepsilon_1 \right) W / \left( 2 \cos \theta \right) \right]$  is the track-directional distance between the centroid of the posterior surface of  $A_2$  and the track turning point,  $\theta = 10.0^{\circ}$  stand for the angle between the direction of track and the horizontal plane,  $T_2 = d_1 - W/2$  indicates the length parallel to the posterior surface of  $B_3$  from its centroid to the rotation axis  $O_2$ ,  $\varphi$  denotes the additional rotational angle of  $B_3$  relative to the track,  $\varepsilon_2$  is the strain of the side tape for tooth 2, W = 4.8mm is the width of the tooth, L = 5.6mm represents the distance between the center of the arc surface of the tooth and its posterior surface, R = 2.4mm is the radius of the arc of the tooth,  $\varepsilon_1$  is the strain of the side tape for tooth 1,  $T_3 = 13.0$ mm is the width of the track

after complete contraction,  $T_4 = (1 + \varepsilon_1)W \cos \theta$  is the horizontal distance between the centroids of the posterior surfaces of  $A_2$  and  $A_3$ , and

 $T_5 = T_3 + (A + d_1)\sin\theta - T_2\sin(\theta + \varphi) + [T_1 + (1 + \varepsilon_1)W]\sin\theta$  represents the vertical distance between the centroids of the posterior surfaces of A<sub>3</sub> and B<sub>3</sub>. Upon solving the system of equations (S1), it is found that the results cannot be expressed as an explicit expression in terms of  $\varepsilon_1$ . Consequently, substituting the parameter values and numerically resolving the system reveal that:

$$\begin{split} \varepsilon_2 &= 25.0\% \rightarrow \varepsilon_1 = 15.6\% \\ \varepsilon_2 &= 15.0\% \rightarrow \varepsilon_1 = 15.0\% \\ \varepsilon_2 &= 0.0\% \rightarrow \varepsilon_1 = 14.4\% \end{split} \tag{S2}$$

Observation (S2) reveals that variations in  $\mathcal{E}_2$  within the permissible range exert negligible influence on  $\mathcal{E}_1$ . It can thus be concluded that the critical threshold value of  $\mathcal{E}_1$  demarcating whether B<sub>3</sub> contacts A<sub>3</sub> remains constant at 15.0%, regardless of the magnitude of  $\varepsilon_2$ . When  $\varepsilon_1 > 15.0\%$ , B<sub>3</sub> contacts with A<sub>2</sub> but remains non-contacting with A<sub>3</sub> (hereafter termed non-simultaneous contact); When  $\varepsilon_1 = 15.0\%$ , B<sub>3</sub> contacts  $A_2$  and initiates contact with  $A_3$  (hereafter termed simultaneous contact); When  $\varepsilon_1$ 15.0%, B<sub>3</sub> not only contacts both A<sub>2</sub> and A<sub>3</sub> but also induces external rotation in A<sub>3</sub> (hereafter termed over-contact). By analogous reasoning, due to the equal status of the bilateral teeth, a similar phenomenon arises under constant  $\varepsilon_1$  conditions: as  $\varepsilon_2$ progressively decreases, the distance between A<sub>3</sub> and B<sub>4</sub> diminishes until contact occurs. Analysis of this scenario yields parallel conclusions, confirming that the critical threshold value of  $\varepsilon_2$  demarcating contact between A<sub>3</sub> and B<sub>4</sub> is likewise invariant at 15.0%, irrespective of  $\varepsilon_1$ . Based on the above analysis, it is revealed that the interlocking modes of the teeth can be categorized into two distinct classes, partitioned by the strain threshold  $\varepsilon_1 = \varepsilon_2 = 15.0\%$ : bilateral equivalent interlocking and bilateral non-equivalent interlocking.

### Supplementary Text 2. Bilateral equivalent interlocking mode

When  $15.0\% < \varepsilon_1 < \varepsilon_2 \le 25.0\%$ , the teeth manifest the bilateral equivalent interlocking mode, as illustrated in Supplementary Figure 3. During regimes ① to ④, B<sub>3</sub> undergoes sequential transitions from non-simultaneous contact to simultaneous contact and subsequently to over-contact, ultimately leading to the elimination of compression between the arc surfaces of B<sub>3</sub> and A<sub>2</sub>. Similarly, in regimes (5) to (8), A<sub>3</sub> transitions from non-simultaneous contact to simultaneous contact and then to over-contact, ultimately leading to the elimination of compression between the arc surfaces of A<sub>3</sub> and B<sub>3</sub>. As the slider continues its motion, A<sub>3</sub> and B<sub>4</sub> undergo internal rotation until reaching regime ②. A<sub>4</sub> and B<sub>4</sub> repeat the contact conditions of A<sub>3</sub> and B<sub>3</sub> in regime (1), and repeat the above processes for interlocking. Both bilateral teeth initiate from non-simultaneous contact and follow identical interlocking processes. When  $0\% \le \varepsilon_1 < \varepsilon_2 < 15.0\%$ , the teeth exhibit a degenerate bilateral equivalent interlock mode. Under this condition, the initial contact condition of B<sub>3</sub> is over-contact, leading to the non-existence of regimes (1) and (2). As the slider moves, when A<sub>3</sub> reaches the position symmetrical to B<sub>3</sub>, its initial contact condition is also over-contact, thus excluding regimes ⑤ and ⑥ from existing. After the teeth inside the slider reach regime (8), with the continuous movement of the teeth, A<sub>4</sub> and B<sub>4</sub> will replace the positions of  $A_3$  and  $B_3$  in regime 3 and repeat the above interlocking process. Referring to Supplementary Figure 3, the interlock process of the teeth degenerates into  $(3) \rightarrow (4) \rightarrow (7) \rightarrow (8) \rightarrow (11)$ .

#### Supplementary Text 3. Bilateral non-equivalent interlocking mode

When  $\varepsilon_1 < 15.0\% < \varepsilon_2 \le 25.0\%$ , the teeth exhibit a bilateral non-equivalent interlock mode, as depicted in Supplementary Figure 3. The initial contact condition of B<sub>3</sub> is over-contact under the condition that  $\varepsilon_1 < 15.0\%$ , so the regimes ① and ② no longer exist. During regimes 3 to 4, B3 transitions from over-contact to the elimination of compression between the arc surfaces of B<sub>3</sub> and A<sub>2</sub>. In contrast, regimes ⑤ to ⑧ exhibit A<sub>3</sub> transitioning sequentially from non-simultaneous contact to simultaneous contact and then to over-contact, ultimately leading to the elimination of compression between the arc surfaces of A<sub>3</sub> and B<sub>3</sub>. As the slider continues its motion, A<sub>3</sub> and B<sub>4</sub> undergo internal rotation until reaching regime ①. A<sub>4</sub> and B<sub>4</sub> repeat the contact conditions of A<sub>3</sub> and B<sub>3</sub> in regime ③, and repeat the above processes for interlocking. It is observed that the bilateral teeth undergo distinct interlocking processes. In essence, this situation represents a degenerate form of Figure 2E, wherein the transition process of B<sub>3</sub> from simultaneous contact to over-contact is omitted. Additionally, when  $0\% \le \varepsilon_1 < \varepsilon_2 = 15.0\%$ , the teeth exhibit a degenerate bilateral non-equivalent interlock mode. Referring to Supplementary Figure 3, the interlock process of the teeth degenerates into  $3 \rightarrow 4 \rightarrow 6 \rightarrow 7 \rightarrow 8 \rightarrow 1$ . Given that  $\varepsilon_2 = 15.0\%$ , A<sub>3</sub> is in simultaneous contact with B<sub>3</sub> and B<sub>4</sub>, regime (5) no longer exists.

Based on the above discussion, the teeth interlocking processes for two tapes with different strain are shown in Supplementary Table 1.

Supplementary Table 1. The interlocking processes of the teeth under the condition that the two side tapes have strains with  $\varepsilon_1 < \varepsilon_2$ 

	Strain value	Interlocking processes
Bilateral	$15\% < \varepsilon_1 < \varepsilon_2 \le 25\%$	$1)\rightarrow2\rightarrow3\rightarrow4\rightarrow5\rightarrow6\rightarrow7\rightarrow8\rightarrow$
equivalent		9
interlocking	$0\% \le \varepsilon_1 < \varepsilon_2 < 15\%$	$\textcircled{3} \rightarrow \textcircled{4} \rightarrow \textcircled{7} \rightarrow \textcircled{8} \rightarrow \textcircled{1})$
Dil . I	$15\% = \varepsilon_1 < \varepsilon_2 \le 25\%$	$(2) \rightarrow (3) \rightarrow (4) \rightarrow (5) \rightarrow (6) \rightarrow (7) \rightarrow (8) \rightarrow (10)$
Bilateral	1.50/	
non-equivalent interlocking	$\varepsilon_1 < 15\% < \varepsilon_2 \le 25\%$	$3 \rightarrow 4 \rightarrow 5 \rightarrow 6 \rightarrow 7 \rightarrow 8 \rightarrow 1$
	$0\% \le \varepsilon_1 < \varepsilon_2 = 15\%$	$\textcircled{3} \rightarrow \textcircled{4} \rightarrow \textcircled{6} \rightarrow \textcircled{7} \rightarrow \textcircled{8} \rightarrow \textcircled{1}$

The criteria for determining the teeth interlock processes under the condition that  $\varepsilon_1 > \varepsilon_2$  follow analogous principles and are not further elaborated here. According to Supplementary Figure 3, the teeth interlocking processes under the condition of  $\varepsilon_1 > \varepsilon_2$  are shown in Supplementary Table 2.

# Supplementary Table 2. The interlocking processes of the teeth under the condition that the two side tapes have strains with $\varepsilon_1 > \varepsilon_2$

	Strain value	Interlocking processes
Bilateral	$15\% < \varepsilon_2 < \varepsilon_1 \le 25\%$	$1) \to 2 \to 3 \to 4 \to 5 \to 6 \to 7 \to 8$
equivalent	$13/6 < C_2 < C_1 \le 23/6$	→9
interlocking	$0\% \le \varepsilon_2 < \varepsilon_1 < 15\%$	$\textcircled{3} \rightarrow \textcircled{4} \rightarrow \textcircled{7} \rightarrow \textcircled{8} \rightarrow \textcircled{1}$
Bilateral non-equivalent interlocking	$15\% = \varepsilon_2 < \varepsilon_1 \le 25\%$	$1 \to 2 \to 3 \to 4 \to 6 \to 7 \to 8 \to 9$
	$\varepsilon_2 < 15\% < \varepsilon_1 \le 25\%$	$1 \rightarrow 2 \rightarrow 3 \rightarrow 4 \rightarrow 7 \rightarrow 8 \rightarrow 9$
	$0\% \le \varepsilon_2 < \varepsilon_1 = 15\%$	$2 \rightarrow 3 \rightarrow 4 \rightarrow 7 \rightarrow 8 \rightarrow 0$

# Supplementary Text 4. Interlocking processes of teeth for two tapes with the same strain.

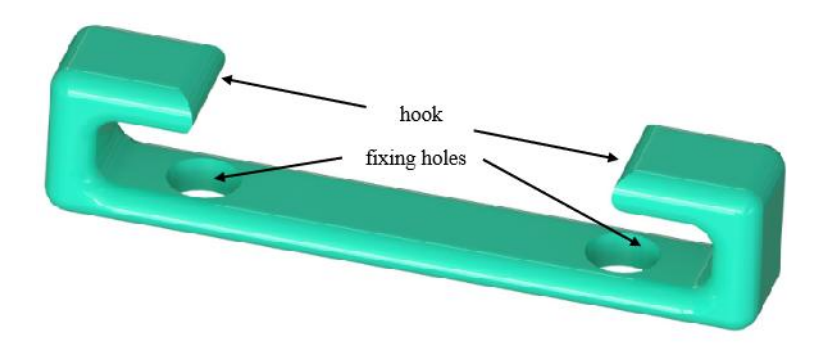
Since the strains of two tapes are the same, the interlocking processes teeth experience on both sides must be the same during zipping. Referring to Supplementary Figure 3, the bilateral equivalent interlocking processes of teeth are shown in Supplementary Table 3.

# Supplementary Table 3. The interlocking processes of the teeth under the condition that the two side tapes have strains with $\varepsilon_1=\varepsilon_2$

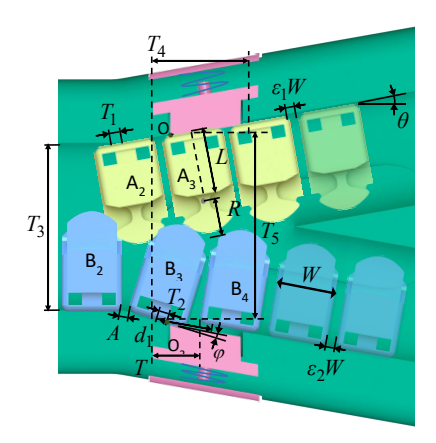
	Strain value	Interlocking processes
		$1) \to 2 \to 3 \to 4 \to 5 \to 6 \to 7 \to 8$
Bilateral equivalent interlocking	$15\% < \varepsilon_1 = \varepsilon_2 \le 25\%$	→⑨
	$\varepsilon_1 = \varepsilon_2 = 15\%$	$2 \rightarrow 3 \rightarrow 4 \rightarrow 6 \rightarrow 7 \rightarrow 8 \rightarrow 10$
	$0\% \le \varepsilon_1 = \varepsilon_2 < 15\%$	$3 \rightarrow 4 \rightarrow 7 \rightarrow 8 \rightarrow 11$

### **Supplementary Text 5. Optimization of slider structure.**

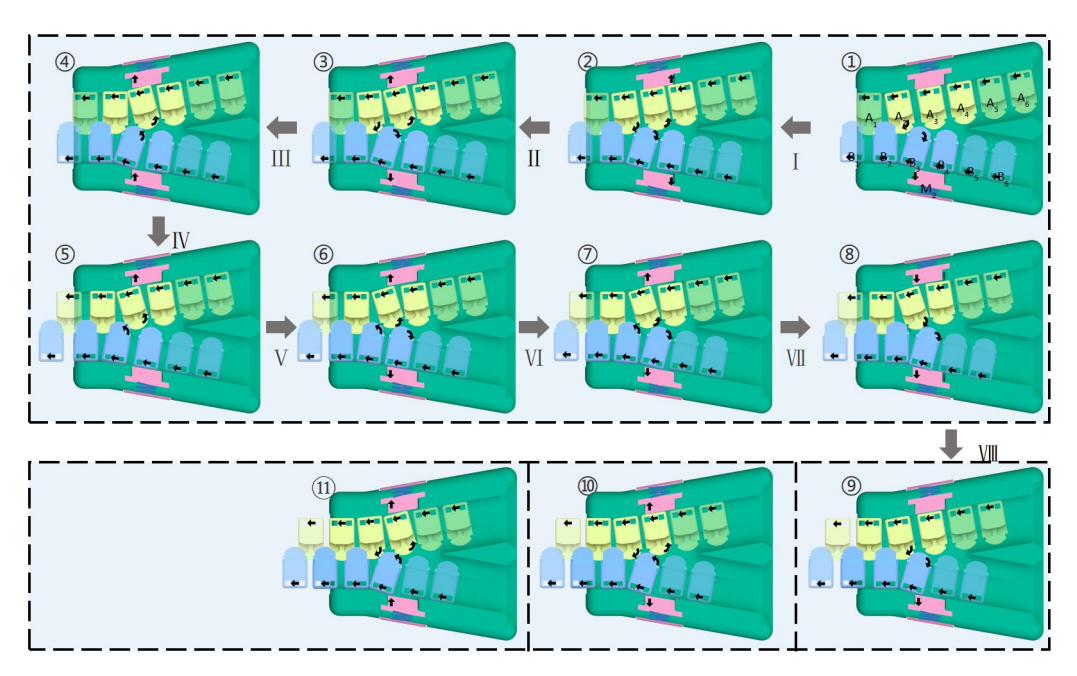
The stretchable zipper must be capable of being zipped with a reasonable zipping force across its full strain range to ensure sufficient practical utility, regardless of the strain difference between its two sides. The position of the movable blocks inside the slider is a critical factor affecting the maximum zipping force of the zipper. Under constant strain conditions of the two tapes, the spatial position of the movable blocks inside the slider influences the rotation axis of the teeth, thereby affecting the difficulty of tooth interlocking. As shown in Supplementary Figure 6A, the track-directional distance between the left end of the front surface of the movable block M2 and the bottom left corner of tooth 2 is denoted as Q. Different values of Q affect the rotation axis of the tooth A<sub>3</sub>'s external rotation. Under constant strain conditions of the two tapes, the moment arm of tooth B<sub>3</sub> acting on the rotation axis O<sub>1</sub> of tooth A<sub>3</sub> decreases as O increases, requiring the slider to apply a greater force to induce external rotation of tooth A<sub>3</sub>. This implies that the maximum zipping force will increase. With reference to the QB/T 2172-2014 industrial standard, the maximum zipping force of the zipper in this design should not exceed 9 N. Considering the complexities of practical application, a 20% redundancy is retained in accordance with general industrial requirements; that is, the maximum zipping force should not exceed 7.5 N. Finite element analysis (FEA) is conducted to determine the maximum zipping force under different strain differences between the two tapes. As shown in Supplementary Figure 6B, when  $Q \le 1.5$  mm, the maximum zipping force of the slider reaches its peak value of 7.5 N at a strain difference of 5%, meeting the redundancy design requirement. Therefore, Q is set to 1.5 mm. At this value, the track-directional distance between the left end of the front surface of the movable blocks and the track turning point, denoted as  $L_{m-t}$ , is 2.6 mm.



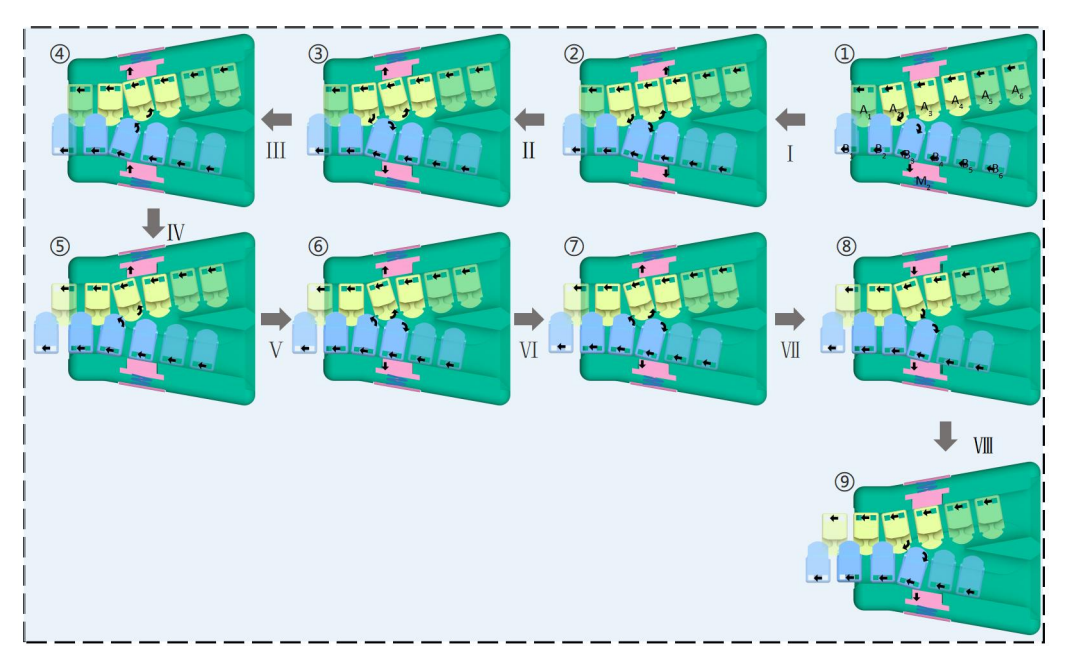
**Supplementary Figure 1.** Hook-furrow stretching limiter.



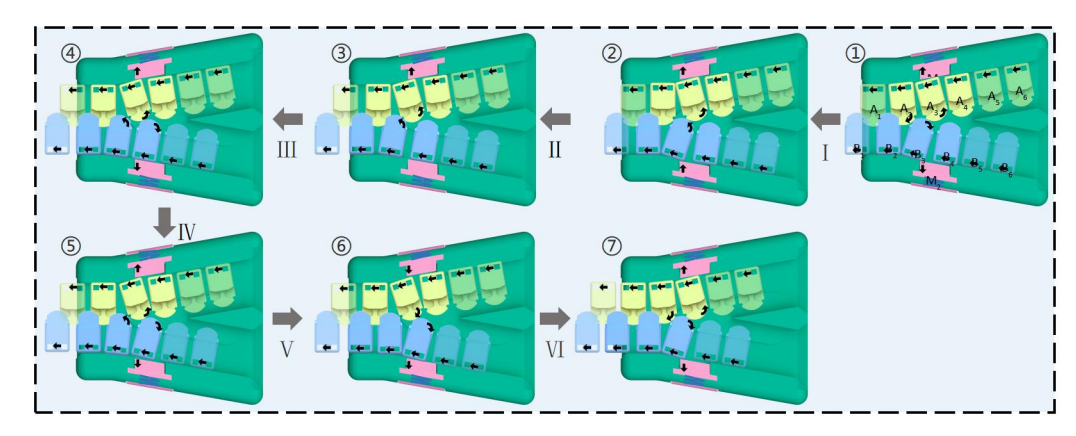
**Supplementary Figure 2.** Initial contact behavior of teeth within the slider during the zipping process.



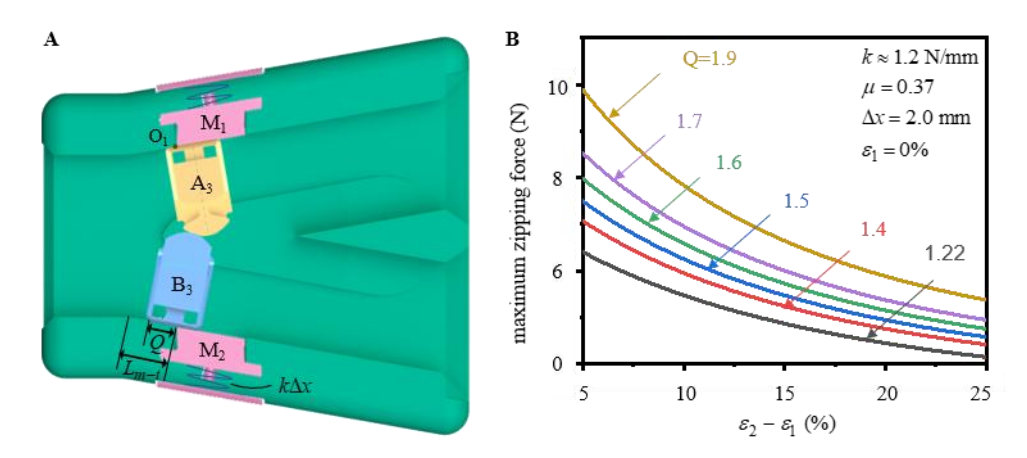
**Supplementary Figure 3.** The interlocking process that the teeth may undergo under conditions  $\varepsilon_1 \le \varepsilon_2$ . The interlocking processes of each pair of teeth sequentially undergo some or all of the regimes from ① to ⑧, depending on different strain values of  $\varepsilon_1$  and  $\varepsilon_2$ . Subsequently, the next pair of teeth replaces the positions of the previous pair and repeats the same interlocking processes. Regime ⑨ represents that  $A_4$  and  $B_4$  replace the positions of  $A_3$  and  $B_3$  in regime ①. Regime ⑩ indicates that  $A_4$  and  $B_4$  replace the positions of  $A_3$  and  $B_3$  in regime ②. Regime ⑪ denotes that  $A_4$  and  $B_4$  replace the positions of  $A_3$  and  $B_3$  in regime ③. The teeth only undergo one of the regimes from ⑨ to ⑪and not in sequence.



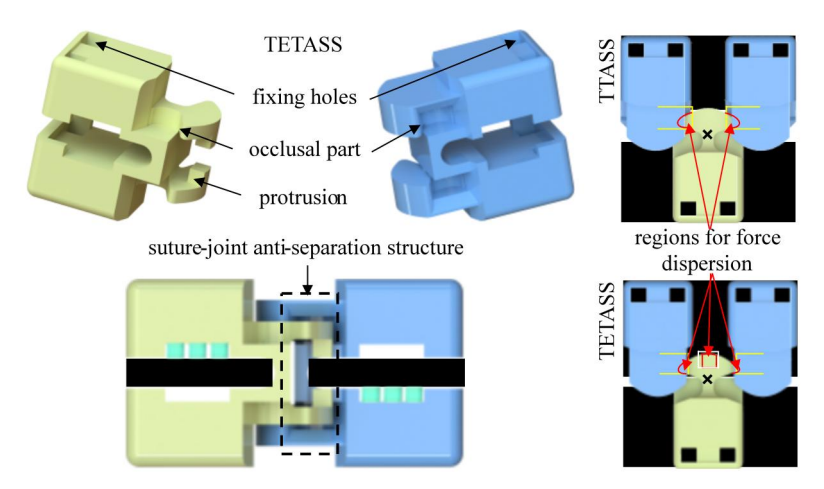
Supplementary Figure 4. A typical bilateral equivalent interlocking mode.



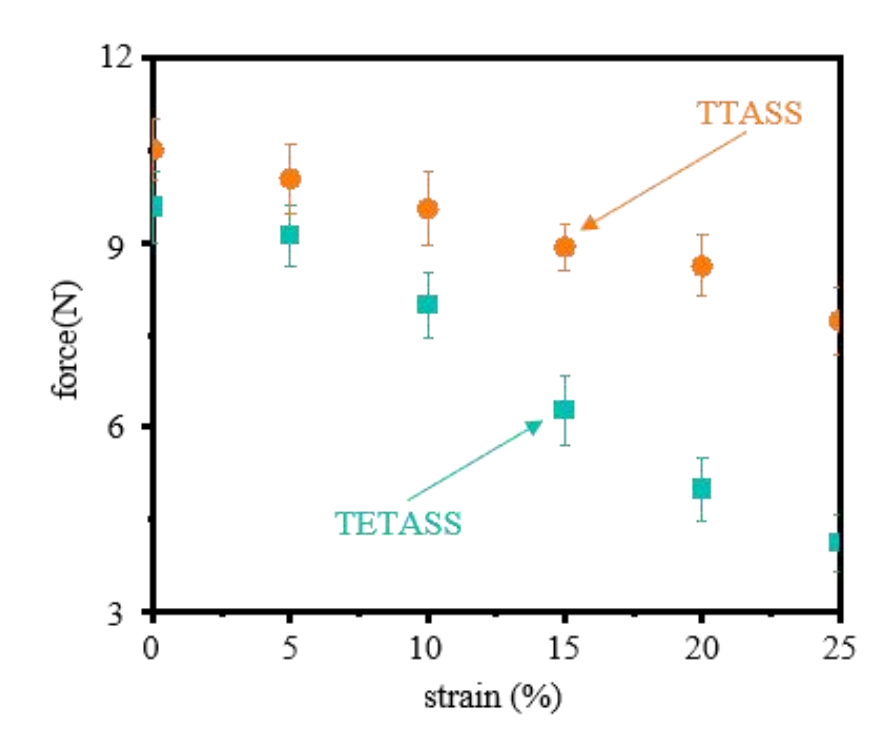
**Supplementary Figure 5.** A typical degenerate bilateral non-equivalent interlocking mode.



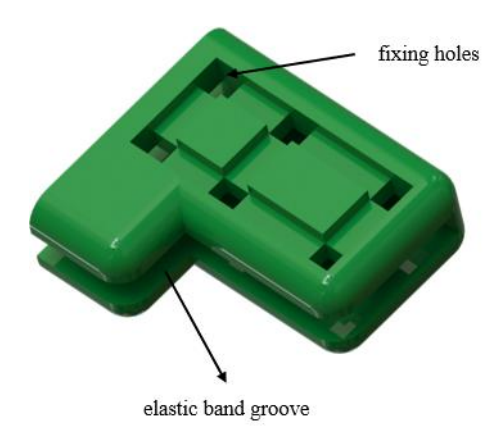
**Supplementary Figure 6.** Slider structure optimization. (A) Spatial positioning of the movable blocks and the interlocking tooth pair within the slider. (B) The maximum zipping force of the zipper under different Q values and strain difference conditions.



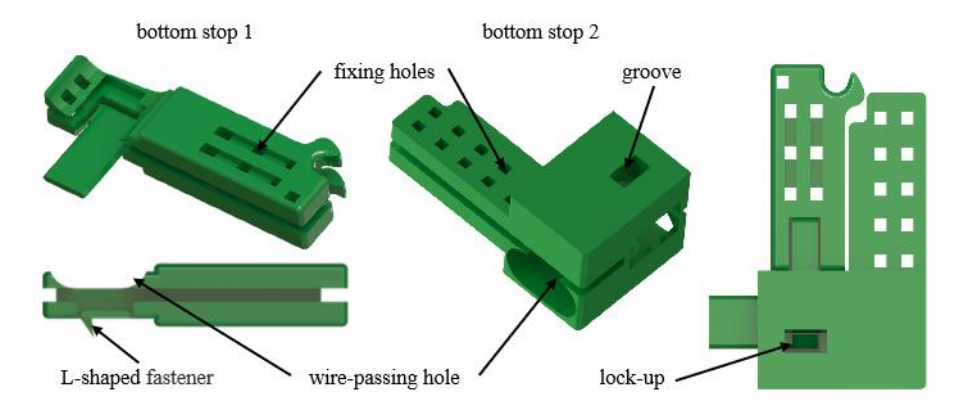
**Supplementary Figure 7.** The specific structure of TETASS and the force dispersion region of TTASS and TETASS.



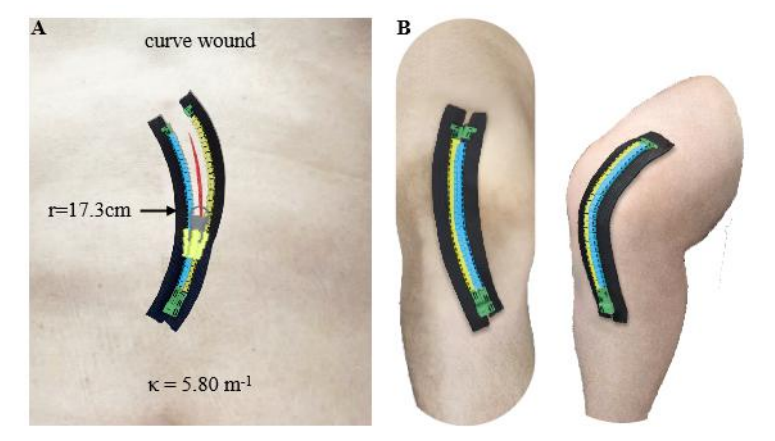
**Supplementary Figure 8.** The anti-separation performance of TTASS and TETASS.



Supplementary Figure 9. The specific structures of top stop.



**Supplementary Figure 10.** The specific structures of bottom stops 1 and 2.



**Supplementary Figure 11.** Application of stretchable zipper in curved wound closure. (A) The thoracoabdominal wound and (B) the knee joint wound.